

## Article

# Strategies for Minimizing Charging Time in Commercial Nickel-Rich/Silicon-Graphite Lithium-Ion Batteries

Jorge Alonso-del-Valle <sup>1,\*</sup>, Manuela González <sup>1</sup>, Juan Carlos Viera <sup>1</sup>, Enrique Ernesto Valdés <sup>2</sup>, Víctor Manuel García <sup>3</sup> and David Anseán <sup>1</sup>

<sup>1</sup> Department of Electrical Engineering, University of Oviedo, 33204 Gijón, Spain

<sup>2</sup> Centro de Investigaciones en Microelectrónica, Facultad de Ingeniería en Telecomunicaciones y Electrónica, Universidad Tecnológica de la Habana “José Antonio Echeverría” (CUJAE), Havana 11500, Cuba

<sup>3</sup> Department of Physical and Analytical Chemistry, University of Oviedo, 33204 Gijón, Spain

\* Correspondence: alonsojorge@uniovi.es

**Abstract:** The emerging nickel-rich/silicon-graphite lithium-ion technology is showing a notable increase in the specific energy, a main requirement for portable devices and electric vehicles. These applications also demand short charging times, while actual charging methods for this technology imply long time or a significant reduction in cycling life. This study analyses the factors that affect the charge behavior for 18,650 commercial nickel-rich/silicon-graphite batteries. For that, long-term cycling tests have been carried out, including electric vehicle standard tests. It can be concluded that this technology has two key issues to develop an efficient charge method: high charge rates should be avoided, mainly below 15% state of charge, and the charge should be finished at 95% of actual cell capacity. This allows that, regardless of application and cell degradation level, cells can be recharged in 2 h without a negative impact on cycling life. For faster charge applications, a new method has been developed to minimize charging time without compromising the cycle life as much as the high current manufacturer method. The proposed fast charge method has proven to be notably faster, recharging in an average 1.3 h (48% less than the high current method and 68% less than the standard method).

**Keywords:** lithium-ion batteries; electric vehicles; fast charge methods; silicon-graphite electrodes; nickel-rich electrodes



**Citation:** Alonso-del-Valle, J.; González, M.; Viera, J.C.; Valdés, E.E.; García, V.M.; Anseán, D. Strategies for Minimizing Charging Time in Commercial Nickel-Rich/Silicon-Graphite Lithium-Ion Batteries. *Batteries* **2022**, *8*, 285. <https://doi.org/10.3390/batteries8120285>

Academic Editor: Carlos Ziebert

Received: 9 October 2022

Accepted: 6 December 2022

Published: 13 December 2022

**Publisher's Note:** MDPI stays neutral with regard to jurisdictional claims in published maps and institutional affiliations.



**Copyright:** © 2022 by the authors. Licensee MDPI, Basel, Switzerland. This article is an open access article distributed under the terms and conditions of the Creative Commons Attribution (CC BY) license (<https://creativecommons.org/licenses/by/4.0/>).

## 1. Introduction

The global demand for energy storage systems with high specific energy has increased in the last years. In particular, the next generation of electric vehicles (EVs) will demand technical improvements in their energy storage systems. Higher specific energy will be required, without compromising the cycle life and the power capability of the energy storage system [1–3].

Among the different energy storage technologies, lithium-ion batteries (LIBs) are one of the most used in a wide range of applications, mainly in the automotive industry, due to their specific energy and power capability. In particular, the market of NMC batteries for hybrid and electric vehicles (EVs) has notably grown in the last few years, due to their high specific energy and high nominal voltage [4].

Moreover, recent studies have shown that new electrode materials can create LIBs with higher specific energy. Mainly, the combination of nickel-rich NMC (nickel-manganese-cobalt) positive electrodes and silicon-graphite negative electrodes can achieve a higher specific capacity than other electrode materials [5–7].

NMC is a composite material that benefits from the technical advantages of its three components. It has a layered atomic structure, similar to lithium-cobalt and lithium-nickel electrodes, which have a high specific energy. The inclusion of manganese allows for a better thermal stability, which is low in cobalt and nickel electrodes [8].

Due to scarcity and price fluctuations of cobalt [9], the industry is moving towards cobalt-free electrodes. For this reason, research in NMC electrodes is focusing on a high nickel ratio, to maintain a high specific energy [9–11].

With regards to the negative electrodes, recent studies have focused on the use of silicon as an electrode material. In theory, pure silicon electrodes have a notably higher specific energy than conventional graphite electrodes, almost ten times higher. However, silicon-based electrodes can suffer important volume changes during lithiation and delithiation, up to 280%, which is not feasible for commercial batteries [12,13]. For this reason, silicon is being used in small quantities along with graphite, forming silicon-graphite electrodes, which have a higher specific energy than pure-graphite electrodes without suffering from notable volume changes [14,15].

Despite the technical advantages of nickel-rich/silicon-graphite batteries in terms of specific energy, the use of this technology in EVs requires a long cycle life, good thermal behavior, and fast charge capability. In recent research, Si-based electrodes show greater capacity fade under cycling than Si-free electrodes [16,17], mainly due to the expansion/contraction of silicon in the negative electrode [18]; also, different degradation modes have been identified in this technology [16–21]. The cycle life could be extended by lowering both the charging cut-off voltage and the charging current rate, or increasing the discharging cut-off voltage [19,20]. However, the reduction of the working voltage range and the charging rate have a negative impact on the final battery charging and discharging performance.

Therefore, it is important to study which factors lead to the cell degradation. In particular, those related to the charging protocol, because they have proven to have a significant impact on cell cycle life, as it will be shown in the paper (Sections 3 and 4). As a result of the analysis, a methodology for developing fast charge methods that fit the application requirements will be proposed and evaluated in Section 5.

## 2. Materials and Methods

### 2.1. Cells and Test Equipment

A batch of 20 commercial cells, LG INR18650-MJ1, were evaluated. The cells' technical specifications from the manufacturer are shown in Table 1. This type of cell has been proven to have a NMC 811 positive electrode and a silicon-graphite electrode. The study from the Munich Technical University was able to measure the electrode composition (82–6.3–11.7% ratio of Ni-Mn-Co at the positive electrode and a 3.5% wt. of Si at the negative electrode) [22]. The main characteristic of these 18,650 cells is the stated capacity of 3500 mAh, notably higher (40%) than the usual capacity of energy cells without nickel-rich/silicon-graphite electrodes (2000–2500 mAh).

**Table 1.** Characteristics of the tested cell (INR18650-MJ1) from the manufacturer (LG Electronics, South Korea).

Parameter	Specification
Nominal Capacity	3500 mAh
Nominal Voltage	3.635 V
Standard Charge	CCCV
CC Current	0.5 C
Constant Voltage	4.2 V
End Current (Cut-Off)	50 mA
Maximum Charge Current	1.0 C
Standard Discharge	0.2 C
Maximum Discharge Current	10 A
Weight	49.0 g
Dimensions	Ø18.4 × 65.0 mm

Before the testing program, all the cells from the batch were submitted to a commissioning protocol and the following conditioning test. The conditioning protocol was based on the United States Advanced Battery Consortium's standard procedures (USABC) [23].

Firstly, the cells were discharged at a C/10 rate until the cut-off voltage stated by the manufacturer (i.e., 2.5 V). After that, several charge-discharge cycles were applied at the following rates: C/3-C/3, C/2-C/2, C/2-C/3, C/2-C/5, and C/25-C/25. Each pair of charge-discharge rates was applied three times except for the C/25 cycle, which was only performed twice. All the charging processes were implemented using a constant current-constant voltage method (CCCV) with the limits stated by the manufacturer: 4.2 V (CC stage) and 50 mA (CV stage).

Regarding the equipment, the test program was performed using an LBT21084 8-Channel Battery Tester (Arbin Instruments, United States); each channel can work with +30/−30 A and 0/+5 V. This system has a 24-bit measurement resolution and a data logging rate of 2000 points/second.

All tests were applied at 23 °C using climate chambers to keep a constant and controlled ambient temperature. Room and cell temperatures are monitored by each Arbin channel via an auxiliary system using T-Type thermocouple sensors.

The test equipment can be seen at the Figure 1: at the right, the Arbin LBT21084 with the auxiliary temperature measurement system, and the connection with the climate chamber; at the top left, the control system. Moreover, some cells under test are shown at the bottom left of Figure 1.



**Figure 1.** Photographs of the test equipment and some cells under test.

Regarding the electrochemical impedance spectrum (EIS) measurements, they were taken with a Gamry Reference 3000 Potentiostat -Gamry Instruments, United States- (current up to 3 A; frequencies from 10  $\mu$ Hz to 1 MHz). In order to isolate the tested cell and minimize possible noise, the system is connected to a Faraday cage placed in a climate chamber (Memmert GmbH, Germany).

## 2.2. Test Program

A test program was designed to evaluate the cells under study, using the following test protocols:

- **Standard charge (C/2) and standard discharge (C/5) rates**, as a cycling evolution reference.
- **Maximum charge rate allowed by the manufacturer (1.0 C) and standard discharge rate (C/5).**

- **Standard charge ( $C/2$ ) and high discharge ( $8\text{ A}$ ;  $2.3\text{ C}$  approx.) rates.**
- **Standard dynamic tests for electric vehicle batteries evaluation: The United States Advanced Battery Consortium's Dynamic Stress Test (USABC, DST) escalated to  $700\text{ W/kg}$  peak discharge power, which is the current USABC target value for electric vehicle batteries at cell level; An adaptation of the European Commission's Worldwide Harmonized Light Vehicle Test Protocol (WLTP), using the standardized speed profile which was translated into a power regime [24], such as the DST test. Figures 2 and 3 show the test profiles, applied to the cells until the cell voltage reaches the lower cut-off voltage stated by the manufacturer ( $2.5\text{ V}$ ). To avoid unsafe operating conditions, both profiles have a current limitation of  $1\text{C}$  for charging (the maximum charge rate stated by the manufacturer).**

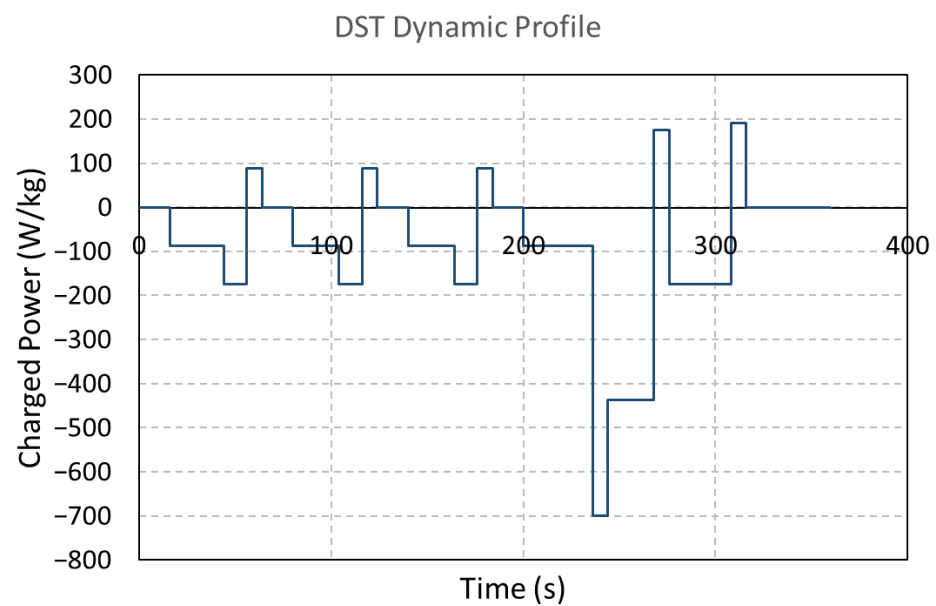


**Figure 2.** USABC Dynamic Stress Test (DST) power profile, escalated to a  $700\text{ W/kg}$  maximum power.

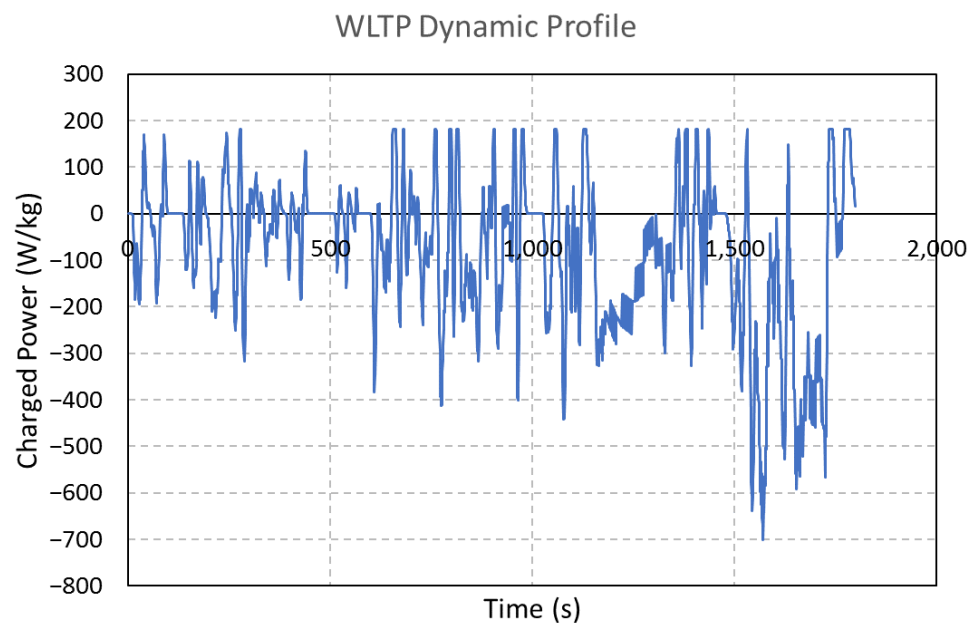


**Figure 3.** Adaptation of the Worldwide Harmonized Light Electric Vehicle Protocol (WLTP), showing the power profile translated from the speed profile and escalated to a  $700\text{ W/kg}$  maximum power.

Overall, five cycling tests were applied to different cells as summarized in Table 2. Note that all tests use the standard CCCV method for charging. DST and WLTP protocols are dynamic tests that involve both charging and discharging; the indicated charge rate is for the charging process applied after the full cell discharge.

**Table 2.** Cycling tests applied to different cells.

Test Type	Charge Rate	Discharge Rate
Standard	C/2	C/5
High Current Charge	C	C/5
High Current Discharge	C/2	8 A (2.3 C approx.)
DST (700 W/kg max)	C/2	DST
WLTP (700 W/g max)	C/2	WLTP

Before starting the cycling tests shown in Table 2, a reference performance test (RPT) was applied. The first step of RPT involved a series of cycles at different charging/discharging rates, to evaluate the cell capacity and the thermal behavior at different power levels. In the second step of RPT, an EIS test was performed on the cell at five different states of charge (5, 20, 50, 80 and 95% of actual cell capacity). The EIS test applied a 50-mA alternate current at different frequencies (from 10 kHz to 10 mHz) and evaluated the cell voltage response, taking 10 measurements/decade.

The RPT was also applied each time that any cell lost 5% of its initial capacity, until the cell capacity was reduced by 20%. In this way, the RPT allowed researchers to monitor the cell state-of-health (SOH) during cycling.

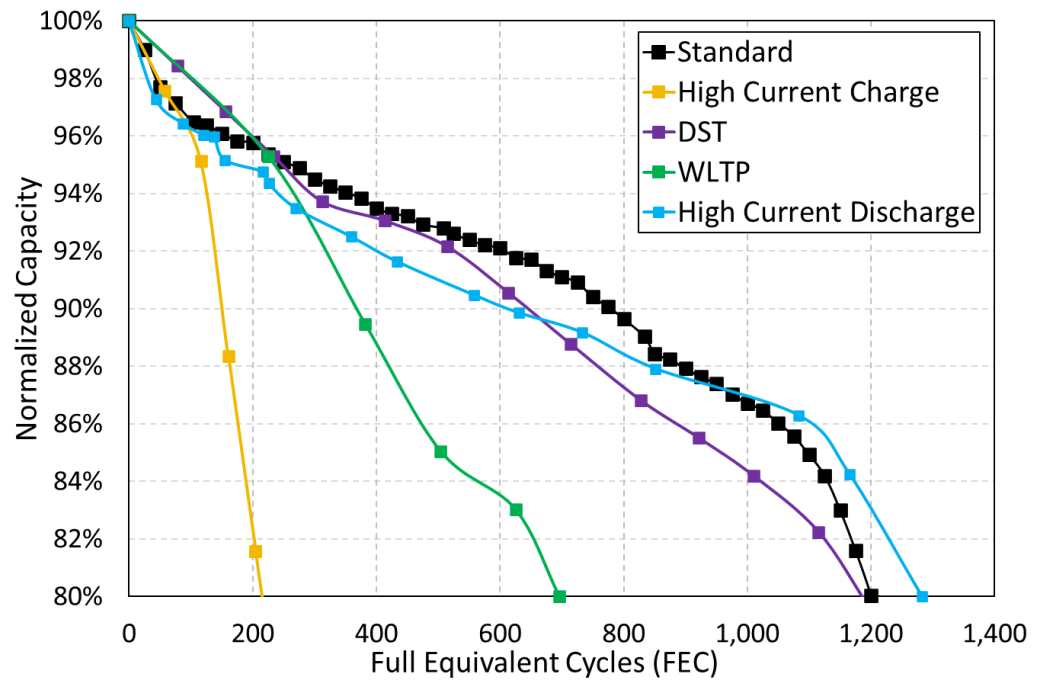
### 3. Cycling Tests Results

The main results of the cycling tests are presented in this section. Firstly, cycle life results indicate how many cycles were completed under each cycling test (see Table 2). Secondly, the charging process is shown in more detail because it is proven that it has the strongest impact on battery life (high rates of regenerative braking and/or charging current); so, this work is focused on optimizing the design of fast charging methods. Finally, electrochemical impedance spectroscopy data represent the cell's dynamic response at different states of charge, showing which ranges have a higher impedance.

#### 3.1. Cycling Life

For a better comparison of results obtained, Figure 4 shows the evolution of cell capacity (under different cycling tests) with the number of full equivalent cycles (FEC). The cell capacity was measured using a standard reference test applied after every 25 cycles, and it was normalized with regard to the fresh cell capacity ( $C_{\text{fresh}}$ , at the first RPT). The FEC were calculated (see Equation (1)) as the total energy throughput  $W_{\text{thr}}$  (total amount of energy discharged during cycling; Wh) divided by the product of the cell nominal voltage  $V_{\text{nom}}$  (V) and the fresh cell capacity  $C_{\text{fresh}}$  (Ah):

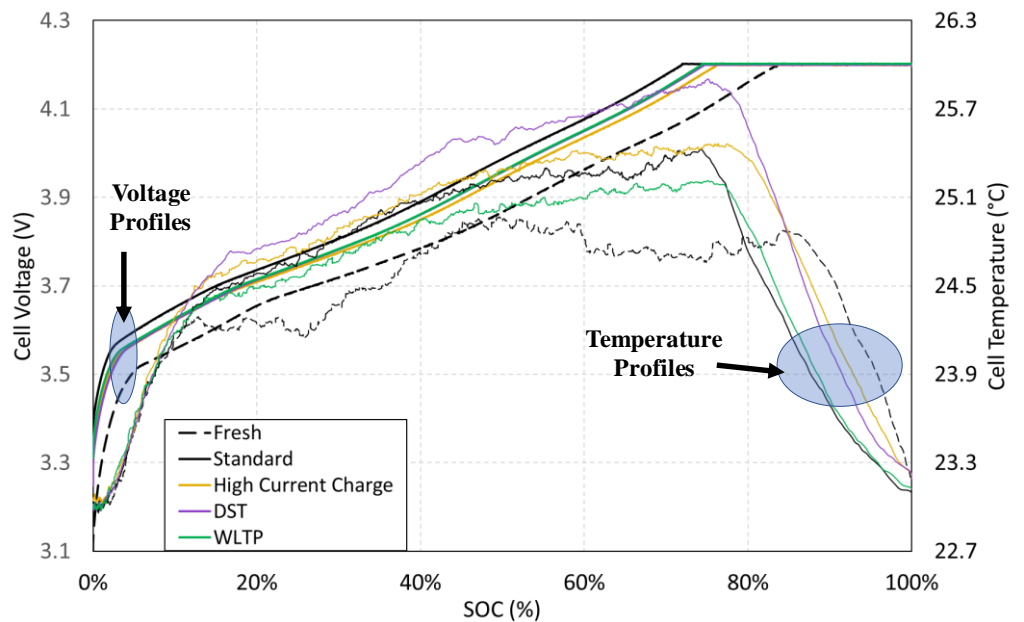
$$\text{FEC} = \frac{W_{\text{thr}}}{V_{\text{nom}} \cdot C_{\text{fresh}}} \quad (1)$$



**Figure 4.** Evolution of normalized cell capacity (under different cycling tests) with the number of full equivalent cycles, calculated as Equation (1).

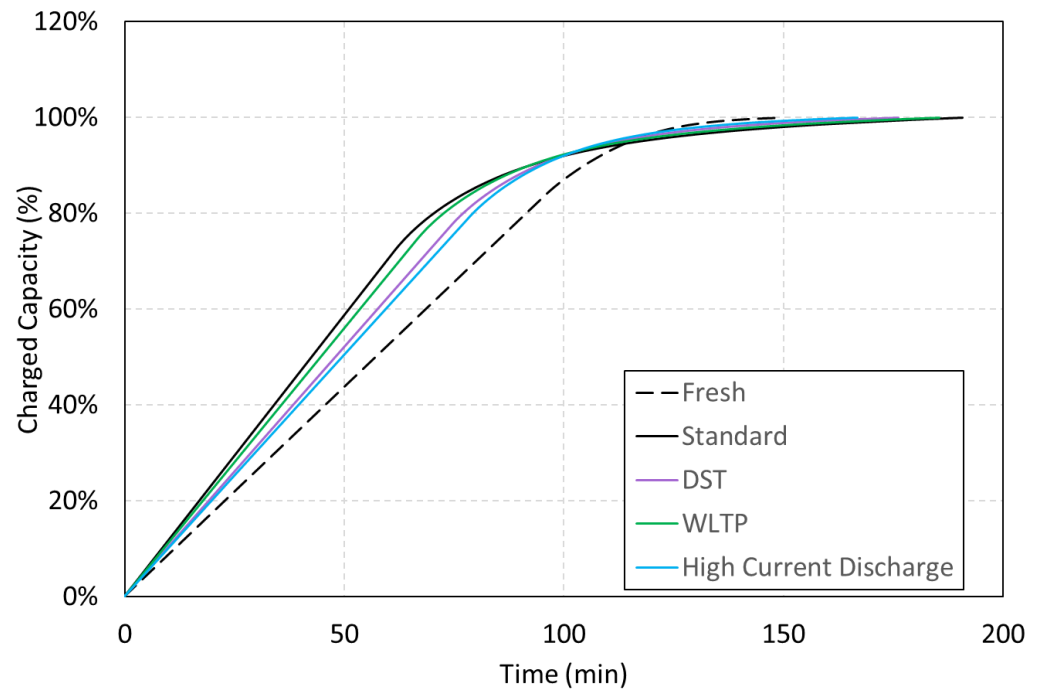
### 3.2. Charging Cell Evolution

Figure 5 shows the standard charge voltage and temperature profiles with regard to the state-of-charge (SOC), for a fresh cell and the different aged cells at 80% SOH.



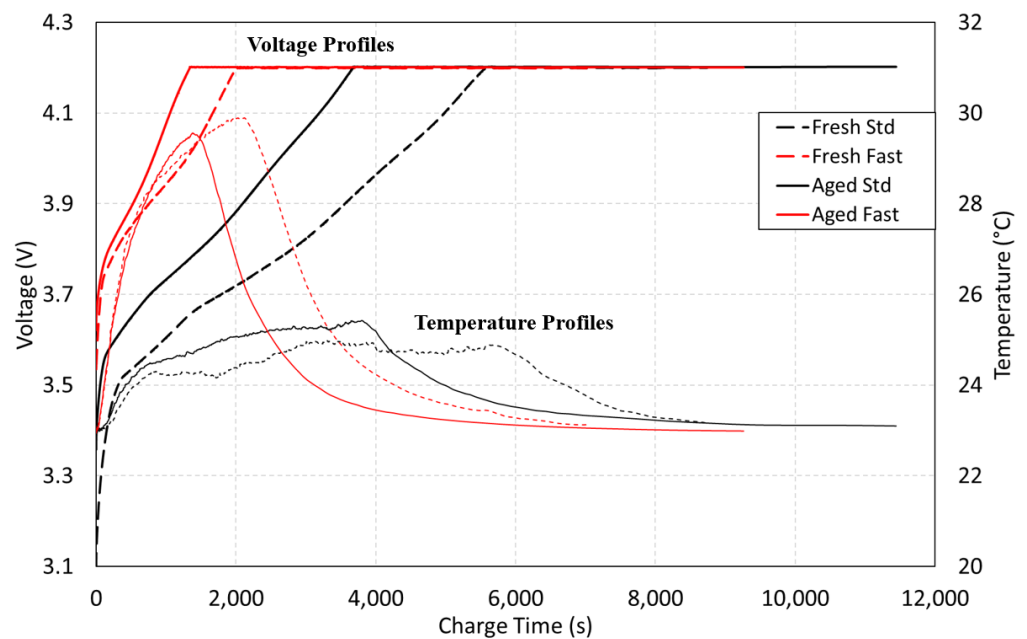
**Figure 5.** Cell voltage and temperature evolution at standard charging for fresh and all cycled cells.

Figure 6 shows the evolution of charged capacity over time for the different cycled cells. The information was taken from a standard cycle during the last RPT of each cell, corresponding to an approximate 80% SOH, and it is shown comparatively to the process in a fresh cell under the same conditions.



**Figure 6.** Evolution of charged capacity over time for a fresh cell and the different cycled cells, under a standard charging process.

Finally, Figure 7 shows charge voltage and temperature profiles over time, for a fresh and a high current charge aged cell, under standard (0.5 C) and high current (1 C) charge methods.



**Figure 7.** Charging process over time, for a fresh and a high current charge aged cell, under standard (0.5 C) and high current (1 C) charge methods.

### 3.3. Electrochemical Impedance Spectroscopy (EIS) Measurements

The EIS technique allows for the measurement of the cell frequency response, which relates to the internal impedance. It also can be used to individually measure the different parts of the cell impedance, such as ohmic resistance, charge transfer and diffusion

resistance. The following figures represent the impedance frequency response of the tested cells, under different states of charge. Figure 8 shows EIS measurements for a fresh cell under 5, 20, 50, 80 and 95% SOC. Since silicon only seems to affect low SOC levels, it is important to precisely measure the cell impedance below 25% SOC [19,25,26]. In this way, Figure 9 shows measurements for the same cell, but under low states of charge (from 5 to 25%, with 5% steps). This information allows researchers to identify which SOC levels have higher impedance values, a key parameter for the design of efficient fast charging methods. Finally, Figure 10 shows the EIS measurements for the standard cycling of an aged cell under the same SOC values as Figure 9 (this EIS is representative of the aged cell's behavior).

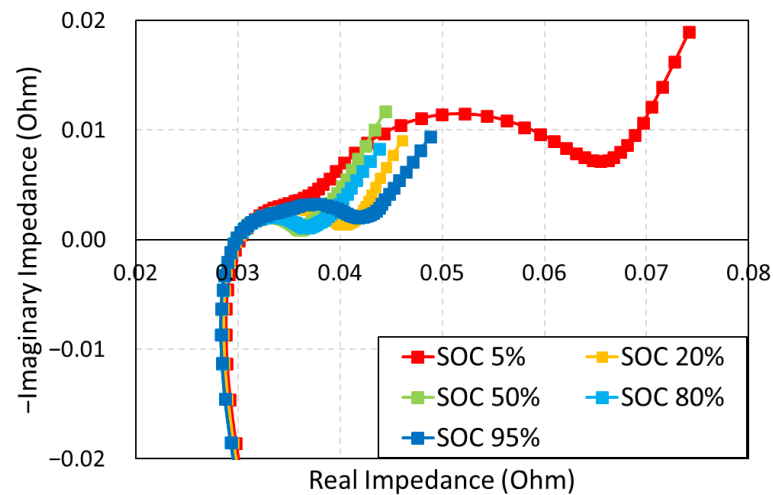


Figure 8. EIS measurements in a fresh cell at 5, 20, 50, 80 and 95% SOC.

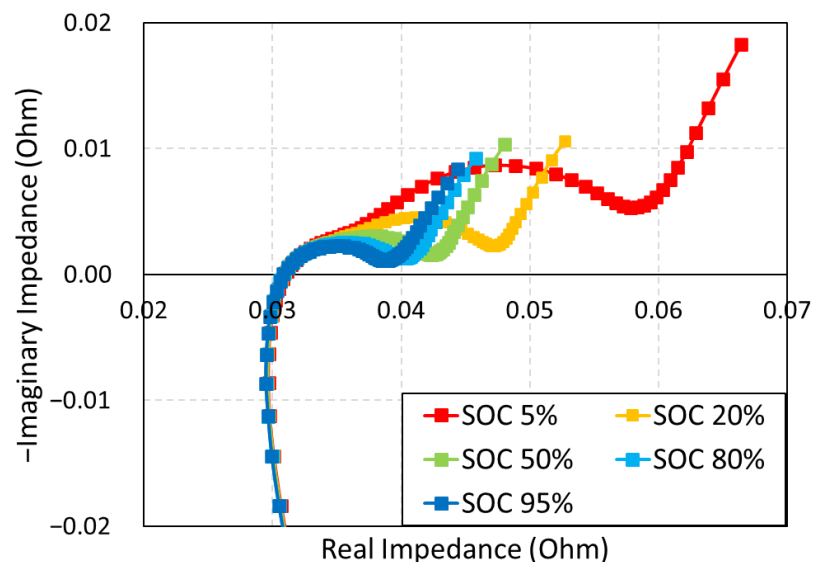
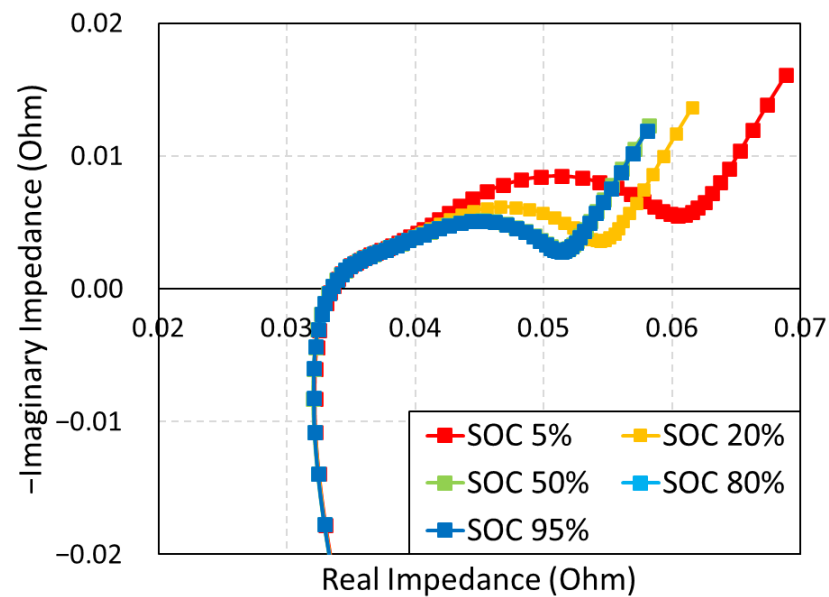


Figure 9. EIS measurements in a fresh cell at 5, 10, 15, 20 and 25% SOC.



**Figure 10.** EIS measurements in an aged cell (80% SOH) at 5, 10, 15, 20 and 25% SOC.

#### 4. Discussion

The main objective of this section is to find the key factors that affect cell performance, mainly regarding the charge process. Based on this analysis, different strategies for minimizing charging time are proposed, including a fast charge method that is described and evaluated in Section 5.

##### 4.1. Cycling Life

The manufacturer states that cells can sustain, under standard working conditions, 80% of its minimum capacity (3400 mAh) for at least 500 cycles. The initial tests on the fresh cells only showed  $3.292 \pm 0.027$  mAh. However, the cells under standard, high current discharge and DST cycling (see Figure 4) were able to achieve more than 1000 full equivalent cycles (FEC) before a 20% reduction in stated minimum capacity (i.e., 2720 mAh).

On the other hand, the cells under high current charge and WLTP cycling show a notably lower cycle life (see Figure 4). Especially, the cell under high current charge cycling has a very short cycle life, with only 220 FEC, which is almost six times lower than the standard cycling. WLTP and DST cycling, as it is shown, respectively, in Figures 2 and 3, emulate regenerative braking applying multiple charge periods during the discharge process. However, the WLTP cycle stresses the cells much more because it applies charge for 487 s (most of the time at 1C limited rate) and the DST for 40 s (around 16 s at 1C). Due to high discharge currents having a slight influence in cycling life, and the WLTP cycling only shows 700 FEC (around 40% less than the DST cycling), it is proven that the use of high charge currents for longer times has a notably negative effect on this type of cell.

Therefore, it can be concluded that the process with the most significant impact on cell cycle life is the charge.

##### 4.2. Charge Analysis

As the charging process has the most significant influence on cell behavior, a detailed analysis is needed. Additionally, this analysis is basic for the design of new charging strategies offering a compromise between charging time and cycling life. For that, the evolution of the main parameters that reveal information about charging process are shown in Section 3.2. (cell temperature, voltage and capacity profiles) and discussed below.

Regarding the temperature, Figure 5 shows the evolution in fresh and aged cells under standard charge. As it can be seen, the increase in the cell surface temperature is not

significant, and it is always lower than 3 °C. The cell internal heat is generated by two sources: ohmic resistance (Joule effect heat) and chemical heat. As the standard charge current is low, the ohmic phenomena only cause a slight heating of cells; so, temperature profiles are a good representation of internal chemical processes.

Looking at the fresh cell profile, different features of interest can be identified. First, a local maximum is detected around 15% SOC (1.5 °C increasing). After that, the temperature remains nearly constant until around 25% SOC. From this, the temperature starts to increase in a linear way until around 50% SOC; at this point, cell temperature reaches the absolute maximum (2.0 °C above ambient temperature). Finally, the temperature keeps almost constant until CV stage is reached (4.2 V), decreasing to ambient temperature during the CV stage.

Looking at aged cell temperature profiles, the shape is similar to the fresh cell, with the main difference that the local maximum is replaced by an inflection point around 15% SOC, going directly to the linear increase stage. In any case, the maximum temperature increasing rate is produced at this first stage. This correlates well with the EIS data, which show a resistance increase at SOC below 15%, as it will be further analyzed on Section 4.3.

From this charge analysis, it can be concluded that the stress is higher on both fresh and aged cells at the first stage (SOC lower than 15%). This behavior in nickel-rich/silicon-graphite lithium-ion technology can be related to the silicon at the negative electrode, more active at low SOC rates [19,25,26].

Figure 6 adds information about charging behavior, showing the relation between charged capacity and charging time. The most interesting result is that all fresh and aged cells reach the 95% SOC at the same time (approximately 120 min) under standard charge. This means that, independently of cycling type and aging state, cells can achieve 95% of their actual capacity in 2 h, with a reduction of total charging time from 22.5% (aged cells at high current discharge cycling) to 38.8% (aged cells at standard cycling).

Finally, Figure 7 shows comparative voltage and temperature evolution over time, in a fresh cell and a high current charge aged cell, when both cells are charged under standard (0.5 C) and high current (1 C) methods. The shape of the temperature profile at each rate is similar for fresh and aged cells, but the values are significantly higher at 1C, reaching the maximum (around 30 °C) at the end of the CC stage. It must be pointed out that the cell temperature increases 3 °C in the first 15% SOC while the rest of the CC stage (from 15% to 60% SOC) only increases by 2 °C. This analysis evidences a higher impedance and a worse cell behavior below 15% SOC, also under high charge currents.

Table 3 shows some important values from Figure 7: the total charge time (CC+CV stages) and the percentage of the CC stage. As it can be seen, the use of 1 C (maximum recommended rate by manufacturer) reduces the charge time with regard to the standard rate (0.5 C): 28% in fresh cells and 19% in aged cells. This difference is due to the notable reduction of the CC stage in aged cells, which increases the CV stage and the total charge time. As it can be seen in Table 3, this effect is stronger at higher charge rates.

**Table 3.** Comparison between the charging behavior of a fresh cell and a high current charge aged cell, when both cells are charged under standard (0.5 C) and high current methods.

Cell Type	Total Charge Time (Minutes)	CC Stage Time (%)
Fresh/Standard Charge Method (0.5 C)	162	52.5%
Fresh/High Current Charge Method (1 C)	117	28.5%
Aged/Standard Charge Method (0.5 C)	190	32.1%
Aged/High Current Charge Method (1 C)	154	14.5%

It must be pointed out that, in this nickel-rich/silicon-graphite lithium-ion technology, the use of high charging rates significantly reduces the charge time but drastically decreasing the cycling life. As it is shown in Figure 4, the cell under the high current charge cycling only completed 220 FEC, while the cell under the standard cycling completed 1200 FEC (82% reduction in cell's service life).

### 4.3. Electrochemical Impedance Spectroscopy

The EIS technique allows researchers to determine the different components of the cell impedance; so, it is widely used for modelling applications [27–30]. However, the EIS has been used in this work only to detect in which SOC zones cell impedance increases.

In this way, Figure 8 highlights the higher impedance at low SOC, especially at 5% SOC, in fresh cells. Due to the relevant influence of cell impedance on charging efficiency, additional tests were carried out on fresh cells at the 0–25% SOC (Figure 9). As it can be seen, the impedance starts to increase significantly below 15% SOC.

EIS measurements were also taken for all aged cells (see an example in Figure 10) and it was verified that the impedance below 15% SOC is always notably higher. This result confirms the conclusions drawn from the charging temperature analysis (Section 4.2), where a sudden increase in the cell temperature is always detected at the first 15% SOC.

## 5. Proposed Fast Charge Method

Reducing the charge time applying high current rates has become an important goal for the widespread use of batteries. However, the behavior of the emerging nickel-rich/silicon-graphite lithium-ion technology has shown that the use of high charge rates significantly decreases the cycle life (see Section 4). For this reason, the objective is to propose a fast charge method that minimizes the charge time without compromising the cycle life as much as the high current method recommended by manufacturer.

Many charge methods have been proposed in the literature for lithium-ion batteries, such as multi-stage charging, pulse charging and variable-current charging [31–35]. One of the most interesting is the multi-stage method, which is similar to the conventional CC–CV method (constant current-constant voltage) but splitting the CC stage into multiple sub-stages at different current rates. In this case, higher currents are used at low-resistance SOC as the cell behaves more efficiently in this zone and the degradation rate is lower. This method has proven to be more efficient than the conventional CCCV method, being able to shorten the charge time and to increase the overall charge efficiency.

The pulse charging consists of a constant current charge that is interrupted by several rest periods. In some cases, short discharge pulses are also applied during the rest periods. This method is helpful for the lithium-ion distribution inside the cell, and it could shorten the charge time and increase the efficiency. However, its implementation in battery management systems (BMS) is complicated, as it needs both controlled charge and discharge pulses, and charging systems are not usually able to perform battery discharge. Furthermore, this method requires a good definition of the duration and intensity of the pulses, and this requires much work on cell modelling and monitoring.

The last alternative that has been analyzed is variable-current charging, which continuously modifies the charge current based on theoretical models of the cell. This method could be able to achieve better efficiency and cycle life than the conventional CCCV method. However, the cell models are non-linear, which implies a high mathematical complexity. Therefore, this method is useful for research purposes, but is hard to implement in real-life applications.

### 5.1. Method Design

Based on the above analysis, the multi-stage charge method has been selected for the design of an efficient fast charge method that is easy to implement in real-life applications. The main point of the method design is to specify how many stages are necessary, and which current rate should be applied in each stage. For that, the following main factors that have been extracted from the analysis of experimental data should be considered:

- (a) The highest cell heating and the highest cell impedance are detected at the same SOC zone (below 15% of actual cell capacity) independently of cell ageing.
- (b) Charging the 100% SOC extends the constant voltage stage and the total charge time, in a greater way as the cell ages. However, a 5% reduction in the total charged capacity significantly decreases the charge time, independently of cell ageing.

Considering these main factors, the following stages and working parameters have been selected for the multi-stage charging method:

- **Stage 1: CC charge at C/2 current rate, until 15% of actual cell capacity.** In this way, the standard charge rate is always applied when the cell impedance is the highest.
- **Stage 2: CC charge at 1C current rate, until 4.2 V.** To reduce charge time notably, the maximum current rate stated by the manufacturer has been selected. Additionally, SOC higher than 15% do not show either a high impedance or thermal phenomenon that clearly increases temperature; so, 1C rate is applied until the maximum voltage is reached.
- **Stage 3: CV charge at 4.2 V, until 95% of actual cell capacity.** In this cell technology, a 5% reduction in the charged capacity significantly decreases the charge time, but hardly affects the final application. On the one hand, the nickel-rich/silicon-graphite technology shows an excellent specific energy, which notably increases the cell capacity (around 40%) compared to the NMC conventional technology. On the other hand, BMS usually stops the charge of Li-ion cells before reaching 100% capacity, in order to reduce CV time and preserve the cycle life.

The proposed fast charge method uses SOC data to define the end conditions of the two charge stages. SOC calculation is one of the main functions of battery management systems (BMS), so SOC data can be easily available for fast charging.

## 5.2. Method Evaluation

The designed fast charge method has been tested and evaluated comparatively with the high current method proposed by cell manufacturer. Table 4 highlights the main charge parameters; the values represent the average behavior of the first 100 cycles under the designed method and the manufacturer's high current method, ended at the same charged capacity of the proposed fast charge method (95% of actual cell capacity).

**Table 4.** Charge parameters of the high current method and the proposed fast charge method.

Parameter	High Current Method	High Current Method (95%)	Proposed Fast Charge Method
Total Charge Time	2.5 h	1.9 h	1.3 h
Discharged Capacity	2.951 Ah	2.803 Ah	2.870 Ah
Maximum Temperature	29.9 °C	29.9 °C	28.4 °C

The proposed fast charge method has proven to be notably faster than the high current method. It is able to charge the cell in an average time of 1.3 h (48% less than the manufacturer method with only 2.7% reduction in discharged capacity). If the same end condition is applied, the proposed method also shows the best performance (32% less time than the manufacturer method with a similar discharged capacity). Moreover, the proposed method is more benign in terms of cell heating (the maximum temperature is reduced by 1.5 °C).

Regarding the cycle life, it must be pointed out that the capacity evolution with cycling is similar in both methods. Therefore, it can be concluded that the proposed method allows to minimize the charging time, without any additional stress on the cell.

However, the use of high charge rates in this technology (see Section 4.2) notably reduces the cell cycle life. Some studies have proven that cut-off voltage values below 4.11 V are able to extend the cycle life [19,20]. Figure 11 shows how much time it is needed in the CV stage of the proposed fast charge method to achieve 90% and 95% SOC, when different cut-off voltage values below 4.2 V were used. Moreover, Figure 12 shows the total charge time for the different cut-off voltage values. In all cases, tests were carried out on fresh cells.

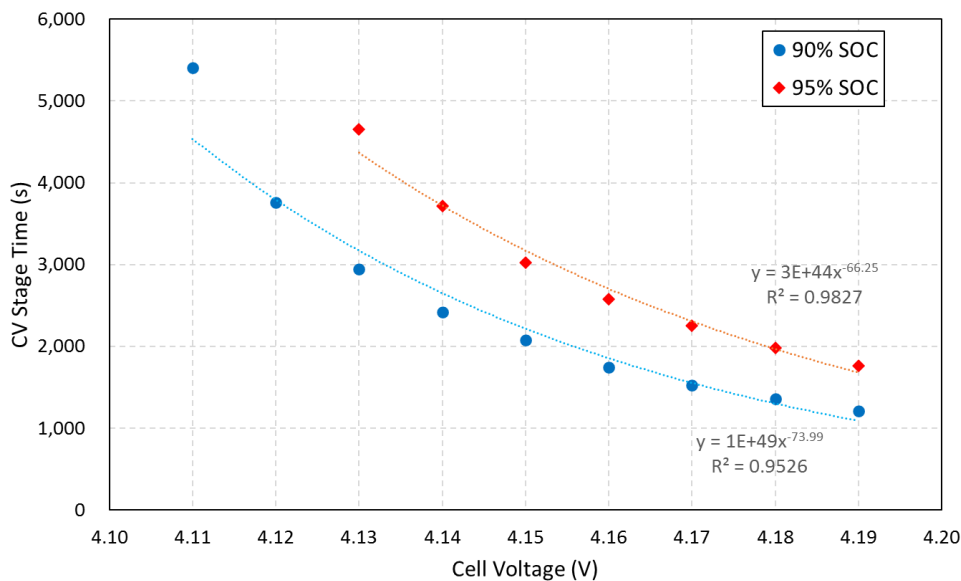


**Figure 11.** Necessary CV stage time at different cut-off voltage values to reach 90% and 95% SOC with the proposed fast charge method. Both data series are fitted to exponential equations, of which the coefficients are also shown.

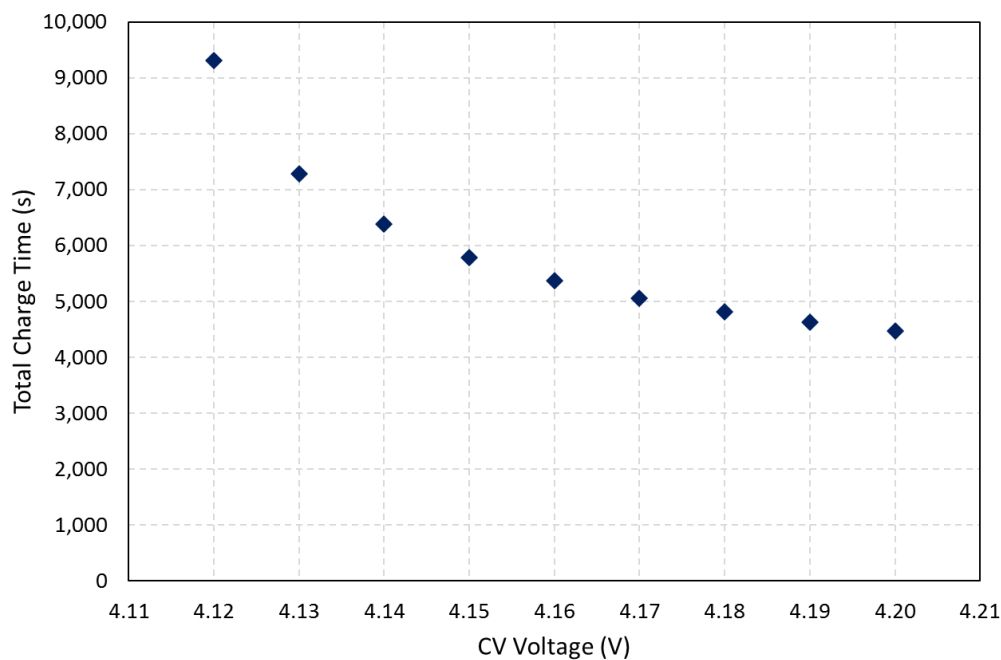


**Figure 12.** Total charge time for different cut-off voltage values below 4.2 V.

As it can be seen in Figure 11, the CV stage time increases exponentially as the cut-off voltage decreases. For this reason, it is possible to slightly reduce the CV voltage without an important increase in the total charge time, as it is shown in Figure 12. For example, reaching 95% SOC using a 4.17 V cut-off voltage requires 1.41 h (an increase of 8.5% compared to 4.2 V).

However, in the case of 4.10 V and 4.11 V, the current reaches the cut-off level (50 mA) even before 90% SOC is achieved. Therefore, cut-off voltage values below 4.11 V could increase cycling life, but they cannot be considered for fast charge methods.

## 6. Conclusions and Future Work

Nickel-rich/silicon-graphite is one of the most promising technologies in the lithium-ion battery market, due to its high specific energy; so, it is expected to be used in the next generation of EVs. For this reason, the performance of this technology under long-term cycling was evaluated, including specific EV profiles involving regenerative braking. The results of this study highlight that the charge process has a significant influence on cycle life. Specifically, the charge methods recommended by cell manufacturers involve either very long charging times or a significant reduction in cycling life.

The detailed study of charging process shows two key issues in developing an efficient fast charge method. Experimental results show that the highest cell heating and the highest cell impedance take place at the same SOC zone (below 15% of the actual cell capacity) regardless of cell ageing. Therefore, it is recommended to avoid cell operation at very low SOC. Moreover, data analysis shows that a small reduction in the total charged capacity (5% of the actual cell capacity) significantly decreases the charge time, in a greater way as the cell ages. Based on those criteria, the proposed fast charge method can significantly reduce the charge time compared to the manufacturer high current method (1.3 h charge time, 48% reduction) without any additional stress on the cell.

On the other hand, the long-term cycling tests highlighted that the use of high charge rates in the nickel-rich/silicon-graphite technology significantly reduces the cell cycle life. Therefore, this technology would need to be enhanced to achieve better acceptance of fast charging. If preserving cycle life is a priority over charging time, it was proved that cells can reach 95% of their actual capacity at a low charge rate (0.5 C) in 2 h, a notable reduction of charging time compared to the standard method, especially for aged cells.

**Author Contributions:** Conceptualization and methodology, J.A.-d.-V., M.G. and J.C.V.; testing, data curation and validation, J.A.-d.-V. and E.E.V.; analysis and investigation, J.A.-d.-V., M.G., J.C.V., V.M.G. and D.A.; writing—original draft preparation, J.A.-d.-V.; writing—review and editing, J.A.-d.-V., M.G. and J.C.V.; supervision, project administration and funding acquisition, M.G. and J.C.V. All authors have read and agreed to the published version of the manuscript.

**Funding:** This research was funded by the Spanish Ministry of Science and Innovation, Spain, via Project PID2019-110955RB-I00/AEI/10.13039/501100011033 and by the Principality of Asturias, Spain via project AYUD/2021/50994, and by Severo Ochoa Program for Predoctoral Scholarships, Spain (PA-18-PF-BP17-134).

**Institutional Review Board Statement:** Not applicable.

**Informed Consent Statement:** Not applicable.

**Data Availability Statement:** Data can be available on request from the article authors: <https://www.uniovi.es/batterylab/contact.htm> (accessed on 22 August 2022).

**Conflicts of Interest:** The authors declare no conflict of interest.

## References

1. Liu, W.; Placke, T.; Chau, K. Overview of batteries and battery management for electric vehicles. *Energy Rep.* **2022**, *8*, 4058–4084. [[CrossRef](#)]
2. Van Mierlo, J. The World Electric Vehicle Journal, The Open Access Journal for the e-Mobility Scene. *World Electr. Veh. J.* **2018**, *9*, 1. [[CrossRef](#)]
3. Feng, S.; Magee, C.L. Technological development of key domains in electric vehicles: Improvement rates, technology trajectories and key assignees. *Appl. Energy* **2020**, *260*, 114264. [[CrossRef](#)]
4. Gandoman, F.H.; Jaguemont, J.; Goutam, S.; Gopalakrishnan, R.; Firouz, Y.; Kalogiannis, T.; Omar, N.; Van Mierlo, J. Concept of reliability and safety assessment of lithium-ion batteries in electric vehicles: Basics, progress, and challenges. *Appl. Energy* **2019**, *251*, 113343. [[CrossRef](#)]
5. Li, H.; Ji, W.; He, Z.; Zhang, Y.; Zhao, J. Distinct capacity fade modes of Nickel-rich/Graphite-SiO<sub>x</sub> power lithium-ion battery. *J. Energy Storage* **2022**, *47*, 103830. [[CrossRef](#)]
6. Zubi, G.; Dufo-López, R.; Carvalho, M.; Pasaoglu, G. The lithium-ion battery: State of the art and future perspectives. *Renew. Sustain. Energy Rev.* **2018**, *89*, 292–308. [[CrossRef](#)]

7. Park, H.; Yoon, N.; Kang, D.; Young, C.H.; Lee, J.K. Electrochemical characteristics and energy densities of lithium-ion batteries using mesoporous silicon and graphite as anodes. *Electrochim. Acta* **2020**, *357*, 136870. [[CrossRef](#)]
8. Blomgren, G.E. The Development and Future of Lithium Ion Batteries. *J. Electrochem. Soc.* **2017**, *164*, 5019–5025. [[CrossRef](#)]
9. Wang, R.; Wang, L.; Fan, Y.; Yang, W.; Zhan, C.; Liu, G. Controversy on necessity of cobalt in nickel-rich cathode materials for lithium-ion batteries. *J. Ind. Eng. Chem.* **2022**, *110*, 120–130. [[CrossRef](#)]
10. Luo, Y.-H.; Wei, H.-X.; Tang, L.-B.; Huang, Y.-D.; Wang, Z.-Y.; He, Z.-J.; Yan, C.; Mao, J.; Dai, K.; Zheng, J.-C. Nickel-rich and cobalt-free layered oxide cathode materials for lithium ion batteries. *Energy Storage Mater.* **2022**, *50*, 274–307. [[CrossRef](#)]
11. Chen, S.; Zhang, X.; Xia, M.; Wei, K.; Zhang, L.; Zhang, X.; Cui, Y.; Shu, J. Issues and challenges of layered lithium nickel cobalt manganese oxides for lithium-ion batteries. *J. Electroanal. Chem.* **2021**, *895*, 115412. [[CrossRef](#)]
12. Liang, B.; Liu, Y.; Xu, Y. Silicon-based materials as high capacity anodes for next generation lithium ion batteries. *J. Power Sources* **2014**, *267*, 469–490. [[CrossRef](#)]
13. Zuo, X.; Zhu, J.; Müller-Buschbaum, P.; Cheng, Y.-J. Silicon based lithium-ion battery anodes: A chronicle perspective review. *Nano Energy* **2017**, *31*, 113–143. [[CrossRef](#)]
14. Goriparti, S.; Miele, E.; De Angelis, F.; Di Fabrizio, E.; Zaccaria, R.P.; Capiglia, C. Review on recent progress of nanostructured anode materials for Li-ion batteries. *J. Power Sources* **2014**, *257*, 421–443. [[CrossRef](#)]
15. Ai, W.; Kirkaldy, N.; Jiang, Y.; Offer, G.; Wang, H.; Wu, B. A composite electrode model for lithium-ion batteries with silicon/graphite negative electrodes. *J. Power Sources* **2022**, *527*, 231142. [[CrossRef](#)]
16. Kalaga, K.; Rodrigues, M.-T.F.; Trask, S.E.; Shkrob, I.A.; Abraham, D.P. Calendar-life versus cycle-life aging of lithium-ion cells with silicon-graphite composite electrodes. *Electrochim. Acta* **2018**, *280*, 221–228. [[CrossRef](#)]
17. Dhillon, S.; Hernández, G.; Wagner, N.P.; Svensson, A.M.; Brandell, D. Modelling capacity fade in silicon-graphite composite electrodes for lithium-ion batteries. *Electrochim. Acta* **2021**, *377*, 138067. [[CrossRef](#)]
18. Bazlen, S.; Heugel, P.; von Kessel, O.; Commerell, W.; Tübke, J. Influence of charging protocols on the charging capability and aging of lithium-ion cells with silicon-containing anodes. *J. Energy Storage* **2022**, *49*, 104044. [[CrossRef](#)]
19. Li, X.; Colclasure, A.; Finegan, D.P.; Ren, D.; Shi, Y.; Feng, X.; Cao, L.; Yang, Y.; Smith, K. Degradation mechanisms of high capacity 18650 cells containing Si-graphite anode and nickel-rich NMC cathode. *Electrochim. Acta* **2018**, *297*, 1109–1120. [[CrossRef](#)]
20. Schindler, M.; Sturm, J.; Ludwig, S.; Durdel, A.; Jossen, A. Comprehensive Analysis of the Aging Behavior of Nickel-Rich Silicon-Graphite Lithium-Ion Cells Subject to Varying Temperature and Charging Profiles. *J. Electrochem. Soc.* **2021**, *168*, 060522. [[CrossRef](#)]
21. Anseán, D.; Baure, G.; González, M.; Cameán, I.; García, A.B.; Dubarry, M. Mechanistic investigation of silicon-graphite/LiNi<sub>0.8</sub>Mn<sub>0.1</sub>Co<sub>0.1</sub>O<sub>2</sub> commercial cells for non-intrusive diagnosis and prognosis. *J. Power Sources* **2020**, *459*, 227882. [[CrossRef](#)]
22. Sturm, J.; Rheinfeld, A.; Zilberman, I.; Spingler, F.B.; Kosch, S.; Frie, F.; Jossen, A. Modeling and simulation of inhomogeneities in a 18650 nickel-rich, silicon-graphite lithium-ion cell during fast charging. *J. Power Sources* **2019**, *412*, 204–223. [[CrossRef](#)]
23. United States Advanced Battery Consortium (USABC). *Electric Vehicle Battery Test Procedures Manual*; USABC: Southfield, MI, USA, 1996.
24. del Valle, J.A.; Viera, J.C.; Anseán, D.; Brañas, C.; Luque, P.; Mántaras, D.; Pulido, Y.F. Design and Validation of a Tool for Prognosis of the Energy Consumption and Performance in Electric Vehicles. *Transp. Res. Procedia* **2018**, *33*, 35–42. [[CrossRef](#)]
25. Yao, K.P.C.; Okasinski, J.S.; Kalaga, K.; Almer, J.D.; Abraham, D.P. Operando Quantification of (De)Lithiation Behavior of Silicon-Graphite Blended Electrodes for Lithium-Ion Batteries. *Adv. Energy Mater.* **2019**, *9*, 1803380. [[CrossRef](#)]
26. Klett, M.; Gilbert, J.A.; Trask, S.E.; Polzin, B.J.; Jansen, A.N.; Dees, D.W.; Abraham, D.P. Electrode Behavior RE-Visited: Monitoring Potential Windows, Capacity Loss, and Impedance Changes in Li<sub>1.03</sub>(Ni<sub>0.5</sub>Co<sub>0.2</sub>Mn<sub>0.3</sub>)<sub>0.97</sub>O<sub>2</sub>/Silicon-Graphite Full Cells. *J. Electrochem. Soc.* **2016**, *163*, A875–A887. [[CrossRef](#)]
27. Skoog, S.; David, S. Parametrization of linear equivalent circuit models over wide temperature and SOC spans for automotive lithium-ion cells using electrochemical impedance spectroscopy. *J. Energy Storage* **2017**, *14*, 39–48. [[CrossRef](#)]
28. Yongming, Y.; Mo, Y.; Quandi, W. Research on High Frequency Model of Hybrid Electric Vehicle Battery. *Res. J. Appl. Sci.* **2013**, *6*, 2601–2606.
29. Korth Pereira Ferraz, P.; Schmidt, R.; Kober, D.; Kowal, J. A high frequency model for predicting the behavior of lithium-ion batteries concerned to fast switching power electronics. *J. Energy Storage* **2018**, *18*, 40–49. [[CrossRef](#)]
30. Fernández Pulido, Y. Characterization and Modeling of Lithium-Ion Cells for Electric Vehicle Applications. Ph.D Thesis, University of Oviedo, Gijón, Spain, 2020.
31. Bandara, T.G.T.A.; Viera, J.C.; González, M. The next generation of fast charging methods for Lithium-ion batteries: The natural current-absorption methods. *Renew. Sustain. Energy Rev.* **2022**, *162*, 112338. [[CrossRef](#)]
32. Wassiliadis, N.; Schneider, J.; Frank, A.; Wildfeuer, L.; Lin, X.; Jossen, A.; Lienkamp, M. Review of fast charging strategies for lithium-ion battery systems and their applicability for battery electric vehicles. *J. Energy Storage* **2021**, *44*, 103306. [[CrossRef](#)]
33. Xie, W.; Liu, X.; He, R.; Li, Y.; Gao, X.; Li, X.; Peng, Z.; Feng, S.; Feng, X.; Yang, S. Challenges and opportunities toward fast-charging of lithium-ion batteries. *J. Energy Storage* **2020**, *32*, 101837. [[CrossRef](#)]
34. Tomaszewska, A.; Chu, Z.; Feng, X.; O’Kane, S.; Liu, X.; Chen, J.; Ji, C.; Endler, E.; Li, R.; Liu, L.; et al. Lithium-ion battery fast charging: A review. *eTransportation* **2019**, *1*, 100011. [[CrossRef](#)]
35. Hemavathi, S.; Shinisha, A. A study on trends and developments in electric vehicle charging technologies. *J. Energy Storage* **2022**, *52*, 105013. [[CrossRef](#)]